

Puzzling accretion onto a black hole in the ultraluminous X-ray source M101 ULX-1

Jifeng Liu¹, Joel N. Bregman², Yu Bai¹, Stephen Justham¹, Paul Crowther³,

¹*Key Laboratory of Optical Astronomy, National Astronomical Observatories, Chinese Academy of Sciences, 20A Datun Rd, Chaoyang District, Beijing, China 100012*

²*Department of Astronomy, University of Michigan, 500 Church St., Ann Arbor, MI 40185, US*

³*Department of Physics & Astronomy, University of Sheffield, Hounsfield Rd, Sheffield S3 7RH, UK*

There are two proposed explanations for ultraluminous X-ray sources^{1,2} (ULXs) with luminosities in excess of 10^{39} erg s⁻¹. They could be intermediate-mass black holes (more than 100-1,000, solar masses, M_{\odot}) radiating at sub-maximal (sub-Eddington) rates, as in Galactic black-hole X-ray binaries but with larger, cooler accretion disks³⁻⁵. Alternatively, they could be stellar-mass black holes radiating at Eddington or super-Eddington rates^{2,6}. On its discovery, M101 ULX-1^{4,7} had a luminosity of 3×10^{39} erg s⁻¹ and a supersoft thermal disk spectrum with an exceptionally low temperature & un-complicated by photons energized by a corona of hot electrons – more consistent with the expected appearance of an accreting intermediate-mass black hole^{3,4}. Here we report optical spectroscopic monitoring of M101 ULX-1. We confirm the previous suggestion⁸ that the system contains a Wolf-Rayet star, and reveal that the orbital period is 8.2 days. The black hole has a minimum mass of $5M_{\odot}$, and more probably a mass of $20 - 30M_{\odot}$, but we argue that it is very unlikely to be

an intermediate-mass black hole. Therefore its exceptionally soft spectra at high Eddington ratios violate the expectations for accretion onto stellar-mass black holes^{9–11}. Accretion must occur from captured stellar wind, which has hitherto been thought to be so inefficient that it could not power an ultraluminous source^{12,13}.

While it is desirable to obtain the primary mass for ultraluminous X-ray sources (ULXs) through measuring the motion of its companion, this is only possible in the X-ray low state because the X-ray irradiated accretion disk will dominate the optical light in the high state^{14,15}. A spectroscopic monitoring campaign for M101 ULX-1 was carried out from February to May 2010 during its expected X-ray low states. The optical spectrum (Figure 1) is characterized by broad helium emission lines, including the He II 4686Å line. Given the absence of broad hydrogen emission lines, which are detected in some ULXs from their X-ray irradiated accretion disk at very high luminosities^{14,15}, the donor cannot be hydrogen rich, and thus must be a Wolf-Rayet (WR) star or a helium white dwarf. The latter can be excluded because a white dwarf is roughly a million times dimmer than the observed optical counterpart even during the low states. Indeed, the optical spectrum is unique to WR stars, and the intensities of the helium emission lines can be reproduced well by an atmospheric model¹⁶ of a WR star, the mass of which is estimated to be $19M_{\odot}$ based on the empirical mass-luminosity relation^{17,18}. Given the relatively low luminosities in the X-ray low state, the helium emission lines are expected to originate mainly from the WR secondary with little contribution from the accretion disk. Such emission lines have been used to measure the black hole (BH) mass in both IC10 X-1 ($21 - 35M_{\odot}$)^{19,20} and NGC300 X-1 ($12 - 24M_{\odot}$)^{21,22}, systems which exhibit luminosities an order of magnitude lower than the peak luminosity of M101 ULX-1.

Since the centroid of the He II 4686Å emission line varied by ± 60 km/s over three months of our monitoring campaign, we have been able to obtain the orbital period of $P = 8.2 \pm 0.1$ days and the mass function $f(M_*, M_\bullet, i) = 0.18 \pm 0.03 M_\odot$ for M101 ULX-1 (Figure 2). Because we already know the mass of the donor star we are able to infer the mass of the accretor to be $M_\bullet \geq 4.6 \pm 0.3 M_\odot$ (for inclination angle $i \leq 90^\circ$), where the error is computed from the uncertainties in the secondary mass and in the mass function. Even for the minimum mass, obtained when the system is aligned perfectly edge-on to the line of sight (for which $i = 90^\circ$), such a compact primary can only be a BH. Higher BH masses are easily obtained for lower inclination angles. For example, a stellar mass BH of $20 M_\odot$ corresponds to $i = 19^\circ$, and an intermediate mass black hole (IMBH) of $1000 M_\odot$ ($300 M_\odot$) corresponds to $i = 3^\circ$ ($i = 5^\circ$). The probability of discovering a pole-on binary with $i < 3^\circ$ ($i = 5^\circ$) by mere chance is lower than 0.1% (0.3%). This makes it very unlikely that this system contains an IMBH of $1000 M_\odot$ ($300 M_\odot$). If the peak luminosity of M101 ULX-1 corresponds to less than 30% of the Eddington level – which is commonly-assumed to be required to produce the thermally-dominated spectral state^{9,23} – then the BH mass would exceed $50 - 80 M_\odot$. The true BH mass seems likely to be $\sim 20 - 30 M_\odot$ (see the Supplementary Information for details).

The confirmation of a WR star in the system, independent of the dynamical mass measurement, also suggests that M101 ULX-1 is unlikely to be an IMBH. IMBHs cannot form directly through the collapse of massive stars, but it is suggested that they can form through mergers in dense stellar environments^{24,25}. However, any IMBH formed would not be seen as a ULX unless they capture a companion as a reservoir from which to accrete matter. Such a capture is a rare

event even in dense stellar environments such as globular clusters or galactic bulges, to which M101 ULX-1 apparently does not belong, and captures that can provide high-enough accretion rates to power a ULX are even more unusual^{26,27}. Given the rarity of WR stars, with roughly 2000 WR stars out of 200 billions of stars in a typical spiral galaxy like the Milky Way¹⁸, it is extremely unlikely that M101 ULX-1 is such a revived IMBH. Alternatively a huge population of IMBHs would somehow remain undetected, both with and without companions.

M101 ULX-1 is thus a stellar black hole, although it is a member of the class of supersoft ULXs which have been considered to be outstanding IMBH candidates^{4,5}. Its combination of high luminosities and low disk temperatures (Figure 3) strains our current understanding of accretion by stellar-mass BHs^{9–11}. Studies of Galactic black hole X-ray binaries suggest that radiation at less than roughly 30% of the Eddington luminosity is dominated by the thermal emission from a hot disk (~ 1 keV). A hard power-law component due to Comptonization by the disk corona becomes more and more significant when the luminosity increases to near-Eddington levels. When the luminosity increases further to Eddington or super-Eddington levels, the Comptonized component begins to dominate over the disk component, as observed for ULXs in the ultraluminous state^{2,6}. For example, the ultraluminous microquasar in M31 with a stellar-mass black hole ($\sim 10M_{\odot}$) and a luminosity of 10^{39} erg s⁻¹ exhibited hard X-ray spectra²⁸. If it were the same phenomenon, a hard X-ray spectra would be expected for a stellar-mass BH in M101 ULX-1, whether it is radiating at sub-, near- or super-Eddington luminosities. The observed supersoft X-ray spectra lack hard photons above 1.5 keV, and can be described purely by cool accretion disks, uncomplicated by Comptonization, with exceptionally low temperatures of 90-180 eV^{4,7}. Including extra pho-

toelectric absorption by the surrounding WR wind into spectral analysis would further lower the underlying disk temperatures and increase the luminosities⁴, which would drive M101 ULX-1 to deviate even farther from the expected hard spectra. This unambiguously demonstrates that stellar mass BHs can have very cool accretion disks uncomplicated by the Comptonized component, contrary to standard expectations^{3,9,11}.

M101 ULX-1 is the third known WR/BH binary but is distinctly different from NGC 300 X-1 and IC 10 X-1. While M101 ULX-1 is a recurrent transient with supersoft spectra and low disk temperatures, both IC 10 X-1 and NGC 300 X-1 show constant X-ray output (despite apparent variations due to orbital modulation), hard spectra with a minor disk component, and disk temperatures above 1 keV^{19,21,29} (Figure 3). Hence the compact object in M101 ULX-1 was considered to be an excellent IMBH candidate, while IC 10 X-1 and NGC 300 X-1 were expected to host stellar mass black holes (as was later confirmed). The 8.2-day orbital period shows that M101 ULX-1 is a wide binary, with components which would be separated by $50R_{\odot}$ for $M_{\bullet} = 5M_{\odot}$ ($75R_{\odot}$ for $M_{\bullet} = 60M_{\odot}$). The Roche lobe radius for the secondary is always greater than $22R_{\odot}$, twice as large as the WR star itself. Mass transfer by Roche lobe overflow is thus impossible, and the black hole must be accreting matter by capturing the thick stellar wind. Given the geometry of the system, the disk is very large, and thus there will be a helium partial ionization zone. Such a disk is prone to instability, causing the observed X-ray transient behaviors for M101 ULX-1. In contrast, IC 10 X-1 and NGC 300 X-1 have shorter orbital periods (34.9 hr and 32.3 hr respectively) and smaller separations ($\sim 20R_{\odot}$). Since those WR stars fill their Roche lobes, the BHs accrete via Roche-lobe overflow. These systems also have much smaller and hotter accretion disks without

helium partial ionization zones, which explains why IC 10 X-1 and NGC 300 X-1 do not display disk-instability outbursts (see also the Supplementary Information).

Mass transfer through wind-accretion usually has a very low efficiency, as in the case of many low-luminosity high mass X-ray binaries, and is typically not considered for populations that require high accretion rates. However, M101 ULX-1 demonstrates that this expectation is not always correct. In particular, transient outbursts of such wind-accreting system have generally not been included in theoretical ULX populations^{12,13}, but M101 ULX-1 does attain ULX luminosities. Theorists have recently suggested that wind accretion may potentially also be significant for some progenitors of type Ia supernovae³⁰. M101 ULX-1 empirically supports this reassessment of the potential importance of wind accretion.

1. Fabbiano, G. The hunt for intermediate-mass black holes. *Science* **307**, 533-534 (2005)
2. Gladstone, J. The sub-classes of ultraluminous X-ray sources. *Conference proceeding from "X-ray Astronomy: towards the next 50 years!" in Milan 2012* astro-ph/1306.6886
3. Miller, J. *et al.* A Comparison of intermediate mass black hole candidate ultraluminous X-ray sources and stellar mass black holes. *Astrophys. J.* **614**, L117-L120 (2004)
4. Kong, A. K. H., Di Stefano, R. & Yuan, F. Evidence of an intermediate-mass black hole: Chandra and XMM-Newton observations of the ultraluminous supersoft X-ray source in M101 during its 2004 outburst. *Astrophys. J.* **617**, L49-L52 (2004)

5. Liu, J.F. & Di Stefano, R. An Ultraluminous Supersoft X-Ray Source in M81: An Intermediate-Mass Black Hole? *Astrophys. J.* **674**, L73-L77 (2008)
6. Gladstone, J. *et al.* The ultraluminous state. *Mon. Not. R. Astron. Soc.* **397**, 1836-1851 (2010)
7. Mukai, K., Still, M., Corbet, R., Kuntz, K. & Barnard, R. The X-ray properties of M101 ULX-1 = CXOKM101 J140332.74+542102. *Astrophys. J.* **634**, 1085-1092 (2005)
8. Liu, J. F. Multi-epoch multi-wavelength study of an ultraluminous X-ray source in M101: the nature of the secondary. *Astrophys. J.* **704**, 1628-1639 (2009)
9. McClintock, J. & Remillard, R. Black hole binaries. *Compact stellar X-ray sources*. Edited by Walter Lewin & Michiel van der Klis. Cambridge Astrophysics Series, No. 39. Cambridge, UK: Cambridge University Press, p. 157 - 213 (2006)
10. Esin, A. A., McClintock, J. E. & Narayan, R. Advection-dominated accretion and the spectral states of black hole X-ray binaries: application to nova MUSCAE 1991. *Astrophys. J.* **489**, 865-889 (1997)
11. Remillard, R. A. & McClintock, J. E. X-ray properties of black-hole binaries. *Annu. Rev. Astron. Astrophys.* **44**, 49-92 (2006)
12. Rappaport, S., Podsiadlowski, Ph. & Pfahl, E. Stellar-mass black hole binaries as ultraluminous X-ray sources. *Mon. Not. R. Astron. Soc.* **356**, 401-414 (2005)
13. Linden, T. *et al.* The Effect of Starburst Metallicity on Bright X-ray Binary Formation Pathways. *Astrophys. J.* **725**, 1984-1994 (2010)

14. Roberts, T. P. *et al.* (No) dynamical constraints on the mass of the black hole in two ULXs. *Astron. Nachr.* **332**, 398-401 (2011)
15. Cseh, D., Grisé, F., Corbel, S. & Kaaret, P. Broad Components in optical emission lines from the ultra-luminous X-ray source NGC 5408 X-1. *Astrophys. J.* **728**, L5-L9 (2011)
16. Hillier, D. J & Miller, D. L. The treatment of non-LTE line blanketing in spherically expanding outflows. *Astrophys. J.* **496**, 407-427 (1998)
17. Schaerer, D. & Maeder, A. Basic relations between physical parameters of Wolf-Rayet stars. *Astron. Astrophys.* **263**, 129-136 (1992)
18. Crowther, P.A. Physical properties of Wolf-Rayet stars. *Annu. Rev. Astron. Astrophys.* **45**, 177C219 (2007)
19. Prestwich, A. H. *et al.* The orbital period of the Wolf-Rayet binary IC 10 X-1: dynamic evidence that the compact object is a black hole. *Astrophys. J.* **669**, L21-L24 (2007)
20. Silverman, J. M. & Filippenko, A. V. On IC 10 X-1, the most massive known stellar-mass black hole. *Astrophys. J.* **678**, L17-L20 (2008)
21. Carpano, S. *et al.* A 33 hour period for the Wolf-Rayet/black hole X-ray binary candidate NGC 300 X-1. *Astron. Astrophys.* **466**, L17-L20 (2007)
22. Crowther, P. A. *et al.* NGC 300 X-1 is a Wolf-Rayet/black hole binary. *Mon. Not. R. Astron. Soc.* **403**, L41-L45 (2010)

23. Steiner, J. F., McClintock, J. E., Remillard, R. A., Narayan, R., Gou, L. J. Measuring black hole spin via the X-ray continuum-fitting method: beyond the thermal dominant state. *Astrophys. J.* **701**, L83-L86 (2009)
24. Miller, M. C. & Hamilton, D. P. Production of intermediate-mass black holes in globular clusters. *Mon. Not. R. Astron. Soc.* **330**, 232-240 (2002)
25. Portegies Zwart, S. F., Baumgardt, H., Hut, P., Makino, J. & McMillan, S. L. W. Formation of massive black holes through runaway collisions in dense young star clusters. *Nature* **428**, 724-726 (2004)
26. Blecha, L. *et al.* Close Binary Interactions of Intermediate-Mass Black Holes: Possible Ultraluminous X-Ray Sources? *Astrophys. J.* **642**, 427-437 (2006)
27. Madhusudhan, N. *et al.* Models of Ultraluminous X-Ray Sources with Intermediate-Mass Black Holes. *Astrophys. J.* **640**, 918-922 (2006)
28. Middleton, M. J. *et al.* Bright radio emission from an ultraluminous stellar-mass microquasar in M31. *Nature*, **493**, 187-190 (2013).
29. Barnard, R.; Clark, J. S. and Kolb, U. C. NGC 300 X-1 and IC 10 X-1: a new breed of black hole binary? *Astron. Astrophys.* **488**, 697-703 (2008)
30. Mohamed, S. & Podsiadlowski, Ph. Mass Transfer in Mira-type Binaries. *Baltic Astronomy*, **21**, 88-96 (2011)

Acknowledgements We thank Drs. Jeffery McClintock, Rosanne Di Stefano, Qingzhong Liu, Xiangdong

Li, Feng Yuan, and ShuangNan Zhang for helpful discussions. J.F. Liu acknowledges support for this work provided by NASA through the Chandra Fellowship Program (grant PF6-70043) and support by National Science Foundation of China through grant NSFC-11273028. The paper is based on observations obtained at the Gemini Observatory, which is operated by the Association of Universities for Research in Astronomy, Inc., under a cooperative agreement with the NSF on behalf of the Gemini partnership: the National Science Foundation (United States), the National Research Council (Canada), CONICYT (Chile), the Australian Research Council (Australia), Ministério da Ciência, Tecnologia e Inovação (Brazil) and Ministerio de Ciencia, Tecnología e Innovación Productiva (Argentina).

Author contributions J.F. Liu and J.N. Bregman proposed the observations, J.F. Liu and Y. Bai reduced the data and carried out the analysis, J.F.Liu, J.N. Bregman and S. Justham discussed the results and wrote the paper, P. Crowther helped to confirm the properties of the Wolf-Rayet star. All commented on the manuscript and contributed to revise the manuscript.

Author information Reprints and permissions information is available at npg.nature.com/reprints. The authors declare that they have no competing financial interests. Readers are welcome to comment on the online version of the paper. Correspondence and requests for materials should be addressed to J.F. Liu (email: jfliu@nao.cas.cn).

Figure 1: The secondary of M101 ULX-1 is confirmed to be a Wolf-Rayet star based on the optical spectrum, combined from 10 Gemini/GMOS observations with a total exposure time of 16 hours. The spectrum shows narrow nebular lines with FWHM of $\sim 4\text{\AA}$ at the instrumental spectral resolution, including hydrogen Balmer lines and forbidden lines such as [OIII] 4960/5006 (the latter is mostly in the CCD gap and only partly shown), [NII] 6548/6583, and [SII] 6716/6731, all at a constant radial velocity over observations consistent with that of M101. Also present are broad emission lines with FWHM up to 20\AA , including strong HeII 4686, HeI 5876, HeI 6679, weaker HeI 4471, HeI 4922, and HeII 5411, and NIII 4640 lines. The observed HeI 5876/HeII 5411 equivalent width ratio suggests a WR star of WN8 sub-type, consistent with the absence of carbon emission lines for WC stars (such as CIII 5696 and CIV 5812). The intensities of the helium emission lines can be best reproduced by an atmospheric model¹⁶ of a Wolf-Rayet star with $R_* = 10.7R_\odot$, $M_* = 17.5M_\odot$, $L_* = 5.4 \times 10^5 L_\odot$, $T_* = 48\text{kK}$, $\dot{M}_* = 2 \pm 0.5 \times 10^{-5} M_\odot/\text{yr}$, $v_\infty = 1300 \pm 100 \text{ km s}^{-1}$ (with 68.3% uncertainties for the two continuously variable parameters), consistent with those for a WN8 star. The mass-luminosity relation^{17,18} for WR stars gives a more reliable mass estimate of $19M_\odot$, which we use in the main text, with an estimated formal error of $1M_\odot$.

Figure 2: An orbital period of ~ 8.2 days is revealed from the radial velocity measurements over three months for M101 ULX-1. The upper panel (a) shows the radial velocities of the HeII 4686Å emission line (with 68.3% uncertainties computed mainly from the dispersion of the wavelength calibration) from nine observations over three months. The lower right panel (b) shows the χ^2 computed for a sine fit (under the assumption of a circular orbit) to the radial velocity curve as a function of trial periods. The trial periods range from a minimum of 3 days, when the WR secondary fills its Roche lobe, to a maximum of 10 days as suggested by the last five measurements. The best fit is achieved at minimal $\chi^2 \sim 1.6$ for $P = 8.2$ days and $K = 61$ km/s, for which the folded radial velocity curve is shown in the lower left panel (c). The 68.3% uncertainties for the best fit are estimated to be $\Delta P = 0.1$ days and $\Delta K = 5$ km/s using $\chi^2 - \chi_{best}^2 = 1$. All other trial periods (such as those at $P \sim 6.4$ days) are worse by $\Delta\chi^2 > 4$. The successful fit with a sine curve suggests that the orbital eccentricity is small. This leads to a mass function $f(M_*, M_\bullet, i) = \frac{PK^3}{2\pi G} = 0.18 \pm 0.03 M_\odot$, where the error accounts for the 68.3% uncertainties in P and K .

Figure 3: The prototype ultraluminous supersoft X-ray source M101 ULX-1 exhibited distinct spectral characteristics. M101 ULX-1 is compared to Galactic black hole X-ray binaries (GBHXRBS), WR/BH binaries IC 10 X-1 and NGC 300 X-1, and other ULXs on the disk X-ray luminosity (L_X) - temperature (T_d) plane, all plotted with the 68.3% uncertainties from the X-ray spectral fitting. Except for M101 ULX-1, which can be fitted with a disk blackbody model with temperatures of 90-180 eV^{4,7}, all other X-ray sources are complicated by the presence of a hard power-law component due to Comptonization by a corona, and can be best fitted with a disk blackbody plus power-law composite model^{3,29}. While GBHXRBS³ and the other two WR/BH binaries²⁹ with stellar black holes cluster in the same region, M101 ULX-1 lies within a distinct region that has been expected to contain IMBH candidates, the same region as for some ULXs³. The dotted lines describe the expected disk luminosity (L_d) for different disk temperatures for a fixed disk inner radius based on the relation $L_d \propto R_{in}^2 T_d^4$. The two lines are offset by 4 orders of magnitudes in luminosity, implying a factor of 100 difference in the disk inner radii, and a factor of 100 difference in the black hole masses if the disk radius is tied to the innermost stable orbit of the black hole. Fitting ULX spectra with alternative Comptonization models can yield high disk temperatures consistent with those of stellar mass black holes⁶. However, the location of M101 ULX-1 on the $L_X - T_d$ plane does not change because its spectra are not complicated by Comptonization at all.

Extended Data Figure 1. M101 ULX-1 as observed in the optical. (a) M101 ULX-1 is located on a spiral arm of the face-on grand-design spiral galaxy M101, as indicated by the arrow. The color image of M101 is composed of GALEX NUV, SDSS g, and 2MASS J images. (b) ULX-1 is identified as a blue object with $V=23.5$ mag at the center of the $1''$ circle on the HST image. The color image is composed of ACS/WFC F435W, F555W and F814W images.

Extended Data Figure 2. Physical properties of the WR secondary from spectral line modeling. Distributions of computed Δ^2 as a function of (a) stellar masses, (b) stellar mass loss rate, (c) stellar radii, and (d) terminal velocity. Here $\Delta^2 = \sum_i (\text{EW} - \text{EW}_i)^2$ computes the difference between observed and synthetic equivalent widths for six broad helium lines present in the Gemini/GMOS spectrum. We have computed synthetic spectra for a group of 5000 real stars from the evolution tracks (as shown by the thick stripes in the mass plot and the radius plot) and for another group of "fake" stars with continuous distributions in mass, radius and luminosity. The best model is labeled by a filled pentagon in all panels.

Extended Data Figure 3. Properties for the Wolf-Rayet/black hole binary for different black hole masses. Shown are the binary separation (solid), the Roche lobe sizes for the Wolf-Rayet star (dotted) and for the black hole (dashed), the capture radius for the black hole when using the terminal velocity (dash-dotted) or when using a simplified velocity law $v(r) = v_\infty(1 - R_*/r)$ (long-short dashed).

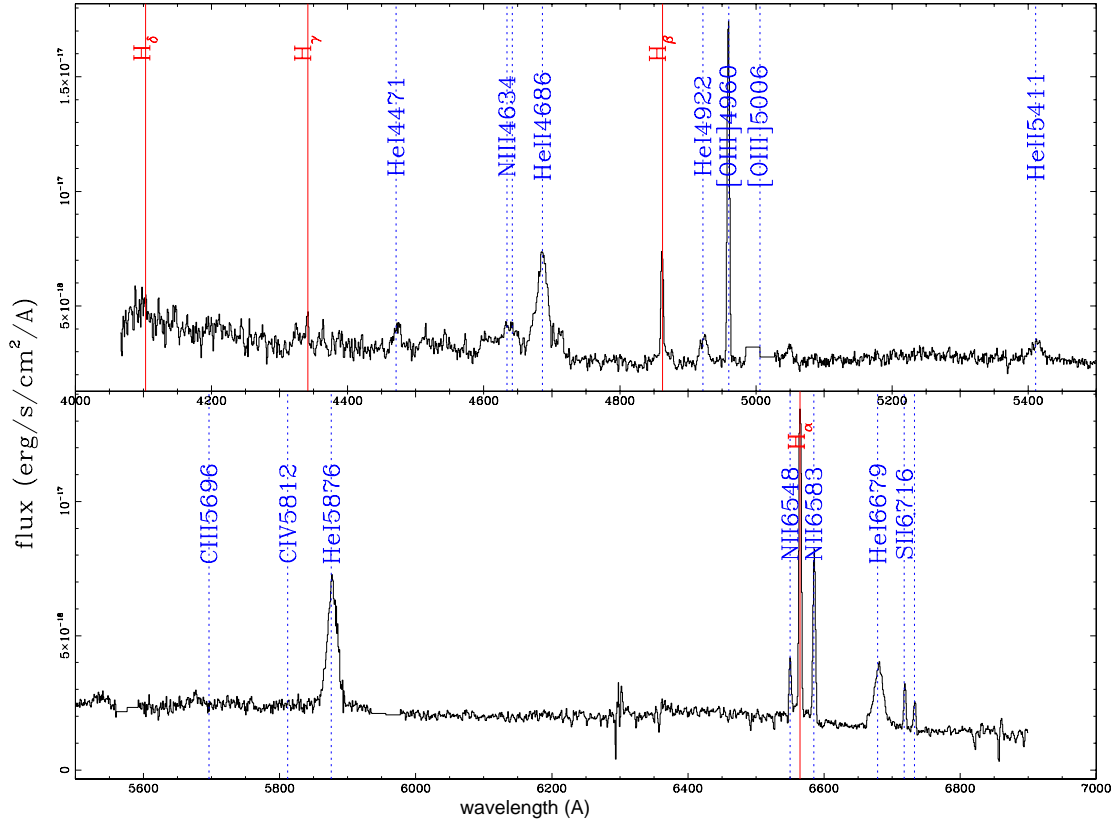
Extended Data Figure 4. The black hole accretion rate for different black hole mass. The accretion rates are computed adopting the terminal velocity (dotted) and a simplified velocity law

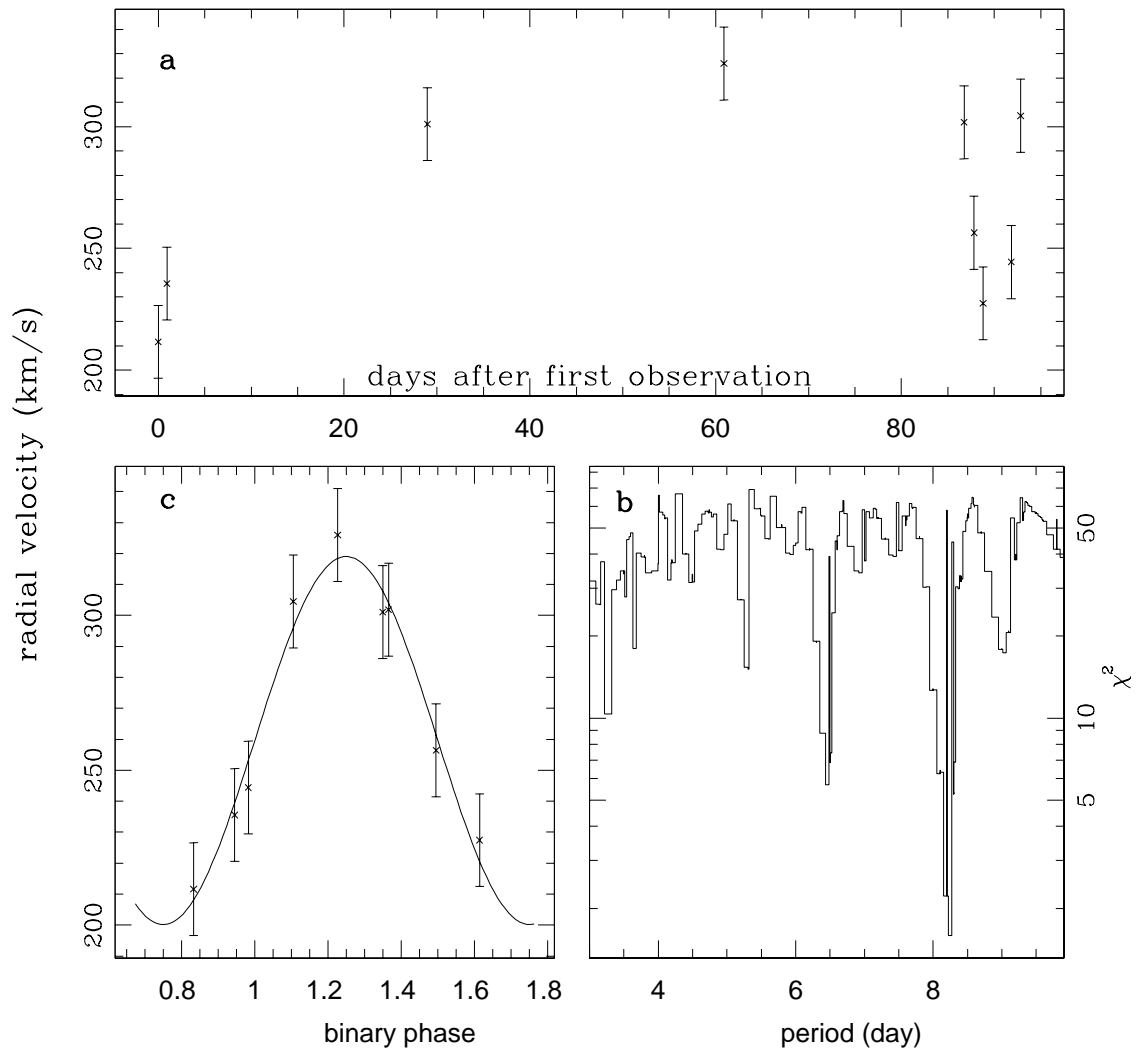
$v(r) = v_{\infty}(1 - R_*/r)$ (solid). To power the observed average luminosity of 3×10^{38} erg/s, the black hole mass must exceed $13M_{\odot}$ ($8M_{\odot}$) using the terminal velocity (the velocity law) for a Kerr black hole, and exceed $46M_{\odot}$ ($28M_{\odot}$) for a Schwarzschild black hole.

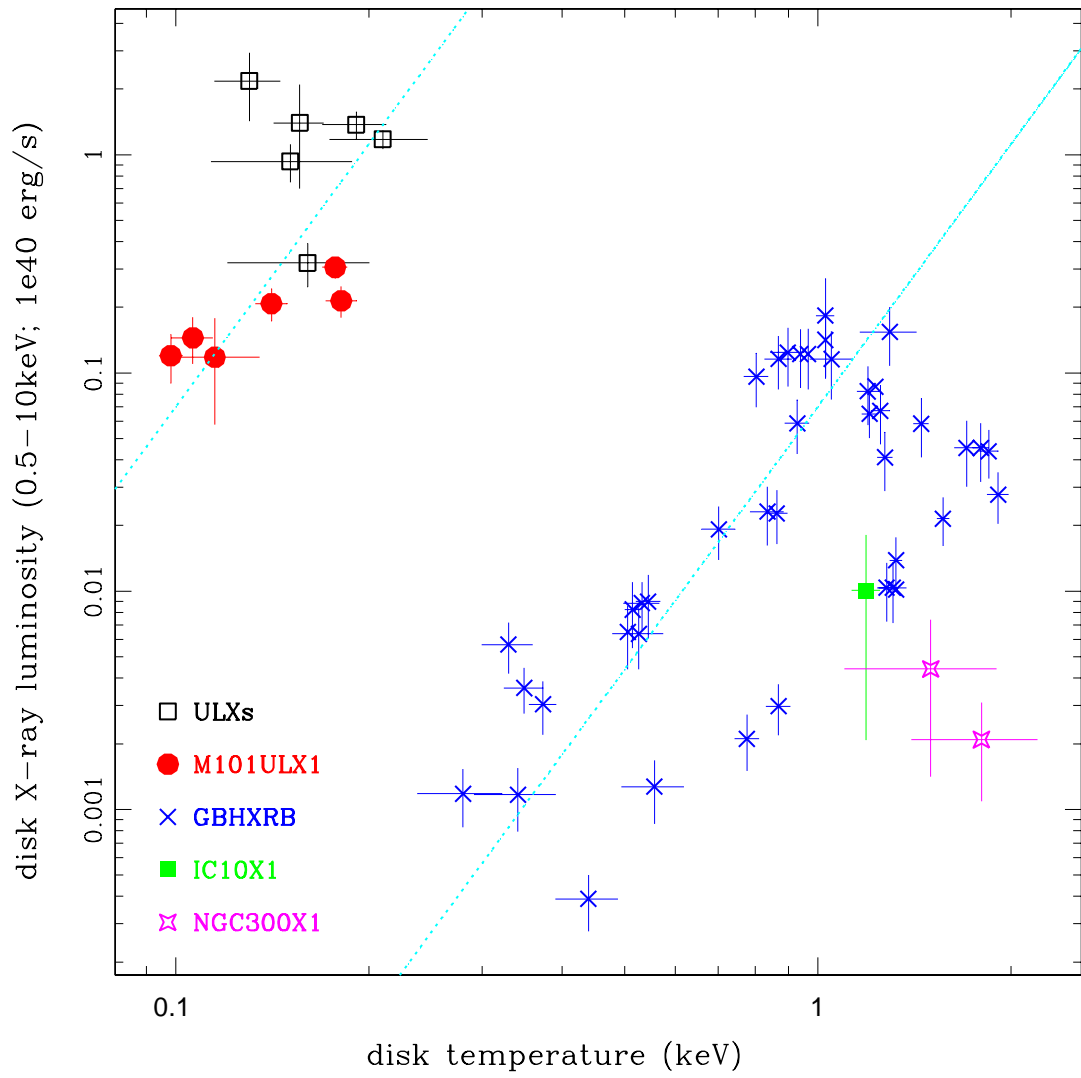
Extended Data Figure 5. Disk temperature structures for M101 ULX-1. (a) The disk temperature profiles for M101 ULX-1 (for $P = 8.24$ days, $M_* = 19M_{\odot}$, $R_* = 10.7R_{\odot}$, $M_{\bullet} = 10/100M_{\odot}$) and NGC300 X-1 (for $P = 32.4$ hr, $M_* = 26M_{\odot}$, $R_* = 7.2R_{\odot}$, $M_{\bullet} = 16.9M_{\odot}$; Crowther et al. 2010). (b) The disk temperature at the outer edge for different black hole mass in M101 ULX-1.

Extended Data Table 1. Gemini/GMOS spectroscopic observations of M101 ULX-1. The columns are: (1) Observation date, (2) Modified Julian Date, (3) exposure time in seconds, (4) barycentric correction computed with `rvsao`, and (5) the corrected radial velocity as measured with HeII 4686, with an error of 15 km/s as mainly from the uncertainties in the wavelength calibration.

Extended Data Table 2. Properties of emission lines. The columns are: (1) emission line ID, (2) FWHM as obtained from Gaussian fit, which equals to 2.35σ , (3) equivalent width, (4) line luminosity in unit of 10^{34} erg/s, and (5) equivalent width from the best WR synthetic model.







Online Methods

This Online Methods part provides details about background information for M101 ULX-1, data reduction and analysis of the Gemini/GMOS spectroscopic observations, search for the orbital periodicity, and properties of the Wolf-Rayet/black hole binary. It contains 5 figures and 2 tables, and additional references.

1 M101 ULX-1 is an outstanding IMBH candidate

M 101 is a nearby face-on grand design spiral galaxy, a frequent target of various observations. These include the optical monitoring observations in search of Cepheids with the Hubble Space Telescope, yielding a distance of 6.855 Mpc³¹. M101 ULX-1 (CXO J140332.3+542103) is located near a spiral arm (Extended Data Figure 1), and identified with a unique optical counterpart of $V = 23.5$ mag³². At this location, the metallicity is $0.4\times$ solar according to the M101 gas-phase oxygen abundance gradient³³.

This ULX has been observed intensively by X-ray missions including ROSAT, XMM and Chandra since early 1990's, which exhibited spectral state transitions between the low-hard state and the high-soft state reminiscent of Galactic black hole X-ray binaries. This ULX was once the brightest X-ray point source in M101 with a Chandra/ACIS count rate of 0.10 count/second³⁴, observed during the 2000 March observation (ObsID 934). The Chandra/XMM-Newton spectra during its outbursts^{4,35} were very soft and can be generally fitted with an absorbed blackbody

model with $n_H = 1 - 4 \times 10^{21} \text{ cm}^{-2}$ and temperatures of 50-100 eV, and the peak 0.3-7 keV luminosity reached $3 \times 10^{40} \text{ erg/s}$, with a bolometric luminosity of about 10^{41} erg/s , suggesting an intermediate mass black holes of a few thousand solar masses. It was argued that it is unphysical to adopt a high neutral absorber column density of $\geq 10^{21} \text{ cm}^{-2}$, and fitting the spectra as blackbody plus a `diskline` component centered at 0.5 keV with N_H fixed at the Galactic value of $4 \times 10^{20} \text{ cm}^{-2}$ yielded the maximum outburst bolometric luminosity of $3 \times 10^{39} \text{ erg s}^{-1}$, consistent with the Eddington luminosity of a black hole of 20-40 M_\odot ⁷.

Even at the lowered luminosities of $3 \times 10^{39} \text{ erg s}^{-1}$, the combination of the disk luminosities and disk temperatures makes M101 ULX-1 an outstanding IMBH candidate. It is believed that the accretion disks for IMBHs should have larger inner radii and consequently lower disk temperatures³⁻⁵, occupying the upper left portion in the $T_{disk} \sim L_X$ plane as shown in Figure 3. The position of M101 ULX-1 on this plane suggests that it is distinctly different from the Galactic BH X-ray binaries in the lower right portion, but belongs to the league of IMBH candidates along with some extreme ULXs above 10^{40} erg/s . The practice of placing these ULXs on this plane was questioned because decomposing ULX spectra into DISKBB+PL is unphysical given the dominance of the hard power-law component. However, in the case of M101 ULX-1 the spectra are supersoft without any hard power-law component, so its location on the plane should reflect the accretion disk uncomplicated by Comptonization. For comparison, we also put on this plane the other two known WR/BH binaries²⁹ IC 10 X-1 and NGC 300 X-1, which apparently belong to the league of stellar mass black holes, and dynamical mass measurements have yielded mass estimates of $20 - 30 M_\odot$.

Combined analysis of 26 HST observations and 33 X-ray observations over 16 years⁸ revealed two optical outbursts in addition to 5 X-ray outbursts. While there is no “exact” period for the recurring outbursts, the outbursts occur once roughly every six months. Such outbursts last 10-30 days, suggesting a outburst duty cycle of 10%-15%. Outside outbursts, ULX-1 stays in a low-hard state with an X-ray luminosity of 2×10^{37} erg/s^{4,7,8,35}. Such behaviors is reminiscent of those of soft X-ray transients in low-mass X-ray binaries, albeit with higher luminosities and lower disk temperatures, but are different from the recently discovered high mass fast transients due to clumping winds at much lower X-ray luminosities ($\sim 10^{34}$ erg/s). Detailed studies of the optical spectral energy distribution, after removal of optical emission from the X-ray irradiated accretion disk in the outbursts, suggest that the secondary is a Wolf-Rayet star of initially 40–60 M_{\odot} , currently 18–20 M_{\odot} , 9–12 R_{\odot} and about 5×10^4 Kelvin⁸. This claim of a WR companion is supported by the presence of the He II $\lambda 4686$ emission line in the Gemini/GMOS-N spectrum taken in 2005³⁶.

2 Gemini/GMOS data reduction

M101 ULX-1 was monitored spectroscopically from February to May in 2010 during its expected low states under the Gemini/GMOS-N program GN-2010A-Q49 (PI: Jifeng Liu). Extended Data Table 1 lists the observations taken in ten nights distributed from February to May, with a total exposure of 15.6 hours. All exposures were taken with the 0.''75 slit and the B600 grating tuned for a wavelength coverage from 4000Å to 6900Å; such a slit/grating combination will yield a spectral resolution of about 4.5Å. We followed standard procedures to reduce the observations and

extract 1-D spectra using the `gmos` package in `IRAF`. All consecutive sub-exposures during one night were combined into one spectrum to increase the signal-to-noise ratio, and we obtained ten spectra with exposure times ranging from 3200 seconds to 9600 seconds (Extended Data Table 1).

For each spectrum, the wavelength solution was obtained using the Copper-Argon arc lamp spectra taken with the same slit/grating setting right before and after the science exposures during the same night or occasionally the night after. We verified the wavelength solution by comparing thus obtained wavelengths to the intrinsic wavelengths for a dozen of strong night sky emission lines identified in the spectra before sky subtraction, and revealed wavelength differences with a dispersion of about 0.25\AA , or $\sim 15\text{ km/s}$. The extracted spectra were converted to flux spectra using the standard star HZ44 taken during the night of February 15, and we scaled the spectra to have $f_{\lambda} = 1.5 \times 10^{-18}\text{ erg/s/cm}^2/\text{\AA}$ at 5500\AA corresponding to $F555W = 23.5\text{ mag}$ based on previous HST/WFPC2 observations⁸.

Figure 1 shows the flux-calibrated sky-subtracted spectrum combined from the ten spectra. The combined spectrum is free of absorption lines but abundant in emission lines as identified and listed in Extended Data Table 2. For each emission line, we fit a Gaussian profile to derive its line width and compute its line flux and luminosity. Two categories of lines are present in the spectrum. The first category is the broad helium emission lines with FWHM of up to 20\AA , five times broader than the instrumental spectral resolution, and includes strong HeII 4686, HeI 5876, HeI 6679, and weaker HeI 4471, HeI 4922, and HeII 5411 lines. The broad NIII 4634 emission line is also present. The second category is the the narrow emission lines with line widths consistent

with the instrumental spectral resolution, and includes the Balmer lines and forbidden lines such as [OIII] 4960/5006 (the latter is mostly in the CCD gap and not listed), [NII] 6548/6583, and [SII] 6716/6731.

The emission line properties are derived from the Gaussian line profile fitting. The average line properties including FWHM, Equivalent Width, and line luminosities are measured from the combined spectrum (Extended Data Table 2). The shifts of the line centers were also measured for individual spectra, with the barycentric correction computed using the `rvsao` package in IRAF as listed in Extended Data Table 1 for each spectrum. It was found that the line shifts, after barycentric correction, are consistent with being constant for narrow emission lines over all observations at 230 ± 15 km/s, consistent with the radial velocity of 241 ± 2 km/s for the face-on M101. However, the broad helium emission lines, as measured with the strongest He II 4686 line, shifted from observation to observation between 210 km/s and 330 km/s as listed in Extended Data Table 1, with an average of 270 km/s that is significantly different from that for nebular lines.

The properties of the nebular lines help to determine the environmental metallicity and the neutral hydrogen column density. $N2 \equiv [\text{NII}]\lambda 6583/H_\alpha$ can be used as an abundance indicator³⁷ with $12 + \log(\text{O}/\text{H}) = 8.90 + 0.57 \times N2$, albeit with a large dispersion in $\log(\text{O}/\text{H})$ of ± 0.41 . Given the equivalent width of these two lines (Extended Data Table 2), we find $12 + \log(\text{O}/\text{H}) = 8.70$, close to solar metallicity (8.66). This is higher than but marginally consistent with the value of $0.4 \times$ solar according to the M101 gas-phase oxygen abundance gradient³³ given the location of ULX-1. The observed Balmer line flux ratios can be used to infer the dust extinction between

the nebula and the observer. In the nebular emission around ULX-1, the intrinsic ratio H_α/H_β is 2.74 in case B for a thermal temperature of $T=20,000\text{K}$ ³⁸. Assuming $E(B-V) = 0.1$ mag, then $A_{6564} = 0.250\text{mag}$, $A_{4863} = 0.360\text{mag}$, $\Delta A = 0.11$ mag, $\Delta H_\alpha/\Delta H_\beta = 1.1$, and reddened $H_\alpha/H_\beta \sim 3$. The observed H_α/H_β is 2.85, suggesting that the extinction is low, and using the Galactic value is reasonable.

3 ULX-1 is a Wolf-Rayet binary of the WN subclass

The broad helium emission lines in the newly obtained Gemini/GMOS spectrum are typical of an extremely hot, hydrogen depleted Wolf-Rayet star. Accretion disks around a compact object can also give rise to broad helium emission lines, but broad Balmer line is expected to be present and much stronger than the helium lines. Indeed, broad H_β emission lines are present in two ULXs with optical spectra (4000-5400Å), NGC1313 X-2¹⁴ and NGC 5408 X-1¹⁵, and are stronger than the He II 4686 emission line. In the ULX-1 spectrum (Figure 1), while the Balmer emission lines are present, they are narrow emission lines like forbidden lines, and should come from the surrounding nebulae, as evidenced by their nearly constant line shifts from observation to observation, in distinct contrast to helium lines with line shift difference of ± 60 km/s.

The sub-type of this Wolf-Rayet star can be determined from the presence or absence of line species in the spectrum¹⁸. There are two main types of Wolf-Rayet stars, WN stars with $R \sim 5 - 12R_\odot$ revealing H-burning products and subsequently more compact WC stars with $R \sim 2 - 3R_\odot$ revealing He-burning products. WC stars are dominant by carbon lines (such as

CIII 4650, CIII 5696 and CIV 5812) that are stronger than helium lines, but none of the carbon lines are present in the ULX-1 spectrum. WN stars from WN4 to WN8 show³⁹ increasing absolute magnitudes M_V from -3.5 mag to -6 mag, increasing mass loss rates from 10^{-5} to $10^{-4} M_\odot/\text{yr}$, decreasing effective temperatures from 80 kK to 45 kK, hence increasing fraction of HeI atoms relative to HeII ions. Comparing the observed spectrum to the spectral atlas of WN stars^{18,40}, we estimate a late-type WN8 star. A WN8 subtype is also inferred based on the HeI 5876/He I 5411 equivalent width ratio⁴¹. Such a subtype is roughly consistent with its absolute magnitude of $M_V = -5.9$ mag (after extinction correction using Galactic $E(B-V) = 0.1$ mag and $R_V = 3.1$), and the effective temperature of about 50 kK derived from its broad-band spectral energy distribution⁸.

4 Physical parameters for the Wolf-Rayet star

As for the case of NGC 300 X-1²², we have calculated synthetic models using the line-blanketed, non-local thermodynamic equilibrium model atmosphere code¹⁶. To select the best physical parameters of the WR star, we compare the model equivalent width with observed values for the six helium emission lines and minimize the quantity $\Delta^2 = \sum_i (\text{EW} - \text{EW}_i)^2$. In all model calculations, elemental abundances are set to 40 percent of the solar value for the metallicity of $0.4Z_\odot$ at the location of ULX-1. We vary the stellar radius R_* between 4 to $20R_\odot$, stellar mass M_* between $5 - 35M_\odot$, stellar luminosity L_* between $5 - 100 \times 10^4 L_\odot$, the outer radius for line-forming region R_{MAX} up to $40R_\odot$, the terminal velocity v_∞ between 400 – 2000 km/s, and the stellar wind mass loss rate \dot{M}_* between $5 - 100 \times 10^{-6} M_\odot/\text{yr}$.

We have run ~ 5000 models with the combination of stellar mass, radius and luminosity determined by the stellar evolution tracks⁴² of $Z = 0.4Z_{\odot}$ for all possible WN stars, and another ~ 5000 models with “fake” stars whose mass, radius and luminosity are completely independent of each other. After a total of ~ 10000 model evaluations, a best fitting model is found with $R_* = 10.7R_{\odot}$, $M_* = 17.5M_{\odot}$, $L_* = 5.4 \times 10^5 L_{\odot}$, $v_{\infty} = 1300$ km/s, $R_{\text{MAX}} = 22R_{\odot}$, and $\dot{M}_* = 2.0 \times 10^{-5} M_{\odot}/\text{yr}$. The model reproduces the helium emission lines extremely well (Extended Data Table 2), with an average difference of $|\Delta| = 0.6\text{\AA}$. In comparison, the majority of models and all models with “fake” stellar parameters are much worse-fitting with $\Delta^2 \gg 10$ (Extended Data Figure 2). Based on the Δ^2 distribution, our model evaluations picked up the stellar parameters effectively, and we estimate, with equivalently $\Delta\chi^2 = 1$, the errors to be $\dot{M}_* = 2 \pm 0.5 \times 10^{-5} M_{\odot}/\text{yr}$, and $v_{\infty} = 1300 \pm 100$ km/s. Note that, if we adopt a solar metallicity, as allowed by the abundance indicator $N2 \equiv [\text{NII}]\lambda 6583/H_{\alpha}$, the best model will change to $R_* = 11.1R_{\odot}$, $M_* = 17.5M_{\odot}$, $L_* = 4.9 \times 10^5 L_{\odot}$, $v_{\infty} = 1700$ km/s, and $\dot{M}_* = 2.4 \times 10^{-5} M_{\odot}/\text{yr}$. This is consistent with the $0.4Z_{\odot}$ results within the errors except for a significantly higher terminal velocity.

The stellar parameters of this best model belong to a “real” WN star from the stellar evolution tracks, with an effective temperature of 48 kK, an initial mass of $42M_{\odot}$, an age of about 5 Myrs, and a remaining lifetime of about 0.3 Myrs before it loses another $\sim 6M_{\odot}$ and collapses into a black hole of $\sim 12M_{\odot}$. This model is actually one of the best models derived from studies of the optical spectral energy distribution⁸. Comparing to the physical properties of WR stars in the Milky Way¹⁸, we find that T_* , L_* , \dot{M}_* , and v_{∞} are consistent with those for a WN7/WN8 star. The

absolute magnitude M_V for ULX-1 ($M_V = -5.9$ mag after extinction correction) is brighter by 0.5 mag, fully within the spread of absolute magnitudes for WN subtypes.

The mass of the WR star can be more reliably estimated with the empirical mass-luminosity relation^{17,18} as done for NGC 300 X-1²². In our case, $L_* = 5.4 \times 10^5 L_\odot$, this corresponds to a WR mass of $19M_\odot$, quite consistent with the mass for the best model. The luminosity derived for solar metallicity will correspond to a WR mass of $18M_\odot$. Hereafter we will use $19M_\odot$ for the WR mass, with an estimated formal error of $1M_\odot$ to roughly reflect the difference between the model value and the empirical value. Given the stellar mass and radius of $10.7R_\odot$, we can obtain the orbital period⁴³ as $P = \sqrt{\rho/110}\text{hr} \simeq 72\text{hr}$ if the WR star is filling its Roche lobe. The true orbital period will be longer than 72 hrs if the WR star is only filling part of its Roche lobe.

5 Search for orbital periodicity

The radial velocity changes between 210 km/s and 330 km/s as measured by the HeII 4686 emission line should reflect the orbital motion of the WR star. While broad HeII 4686 emission line can be produced from the X-ray heated accretion disk in some ULXs with rather high X-ray luminosities (e.g., in NGC 1313 X-2 with $\sim 10^{40}$ erg/s¹⁴), this should not be the case for M101 ULX-1 because its X-ray luminosities during the Gemini/GMOS observations were three orders of magnitude lower, and the disk heating effects are insignificant even in its outburst based on the optical studies⁸. In addition, the line ratios for the heated accretion disk are different from the line ratios for the WR star because the emission line forming regions and temperature structures are

quite different, yet the observed line ratios can be well reproduced by the WR star.

In order to search for the orbital periodicity, we assume a circular orbit and fit a sine curve $v_r = v_0 + K \sin[2\pi(t - t_1)/P + \phi]$ to nine barycenter-corrected radial velocities; the radial velocity for March 17th was dropped from the analysis because the spectrum had a very low signal-to-noise ratio. The four parameters are the radial velocity of the binary mass center v_0 , the radial velocity semi-amplitude K , the orbital period P , and phase ϕ at the first observation. The search is carried out by minimizing χ^2 defined as $\chi^2 = \sum_{i=1}^{10} [v_r(t_i) - v_{r,i}]^2 / \sigma_{v_{r,i}}^2$. The radial velocity errors $\sigma_{v_{r,i}}$ are taken as the wavelength calibration error of 0.25 Å, or 15 km/s. The five radial velocity measurements from May 13th to May 19th suggest a period no longer than 10 days (Figure 2). The amoeba technique is used for χ^2 minimization, using initial guesses taken from the parameter grids with P from 3 to 10 days in step of 0.01 days, K from 20 to 150 km/s in step of 5 km/s, and ϕ from 0° to 360° in step of 10°. The best solution is found at the minimum $\chi^2 = 1.6$, for which the best period $P = 8.24 \pm 0.1$ days and the best radial velocity semi-amplitude $K = 61 \pm 5$ km/s, with the 68.3% error determined with $\Delta\chi^2 = 1$. The fact that the radial velocity curve can be fitted with a sine curve suggests that the orbital eccentricity is small.

Given P and K , the mass function for M101 ULX-1 can be computed as $f(M_*, M_\bullet, i) = \frac{PK^3}{2\pi G} = \frac{M_\bullet^3}{(M_\bullet + M_*)^2} \sin^3 i = 0.178 M_\odot$. This sets an absolute lower limit for the mass of the primary. In the case of ULX-1, more information can be extracted because we already know $M_* = 19 M_\odot$. Given the equation $\frac{M_\bullet^3}{(M_\bullet + M_*)^2} \sin^3 i = 0.178 M_\odot$, the primary mass will increase monotonically when the inclination angle decreases, i.e., changing from edge-on ($i = 90^\circ$) toward face-on ($i =$

0°). Thus the minimum mass for the primary can be obtained when $i = 90^\circ$, which is $M_\bullet = 4.6M_\odot$ after solving the equation $\frac{M_\bullet^3}{(M_\bullet + M_*)^2} = 0.178M_\odot$. The minimum mass will be $M_\bullet = 4.4M_\odot$ if we use $M_* = 17.5M_\odot$. Such a compact primary can only be a black hole. This is thus the dynamical evidence for a black hole in a ULX.

6 The Wolf-Rayet/black hole binary properties

This section duplicates some text from the main article, but with additional technical details.

M101 ULX-1 is thus a Wolf-Rayet/black hole binary, only the third discovered so far after IC 10 X-1 and NGC300 X-1. The binary separation can be computed with Kepler's Law $a^3 = \frac{G(M_* + M_\bullet)}{4\pi^2} P^2$, which increases monotonically for increasing black hole mass, starting from $a = 50R_\odot$ for $M_\bullet = 4.6M_\odot$ to $a = 75R_\odot$ for $M_\bullet = 60M_\odot$ (Extended Data Figure 3). The Roche lobe size for the secondary can be computed with $R_{cr} = a \cdot f(q) = a \cdot 0.49q^{2/3} / [0.6q^{2/3} + \ln(1 + q^{1/3})]$ with $q = M_*/M_\bullet$, and the Roche lobe size for the black hole can be computed with the same formula but with different $q = M_\bullet/M_*$. As shown in Extended Data Figure 3, the Roche lobe size for the black hole increases with the increasing black hole mass, but the Roche lobe size for the secondary does not change much, from $R_{cr,*} = 25R_\odot$ for $M_\bullet = 4.6M_\odot$ to $R_{cr,*} = 23R_\odot$ for $M_\bullet = 10M_\odot$, and to $R_{cr,*} = 22R_\odot$ for $M_\bullet = 20M_\odot$.

Regardless of the black hole mass, the secondary is filling only half of its Roche lobe by radius, and the black hole must be accreting from the Wolf-Rayet star winds. Since the black hole is at least $50R_\odot$ away from the WR star, the stellar wind must have reached close to its

terminal velocity. The capture radius for the wind accretion can be computed as $r_{acc} = \frac{2GM_{\bullet}}{v_{\infty}^2}$, and the accretion rate can be computed as $\dot{M}_{\bullet} = \frac{\pi r_{acc}^2}{4\pi a^2} \dot{M}_{*}$. Given that the average luminosity for M101 ULX-1 is about 3×10^{38} erg/s, the required accretion rate is $\dot{M}_{\bullet} = L/\eta c^2 \simeq \frac{L_{38}}{\eta} 2 \times 10^{-9} M_{\odot}/yr = \frac{1}{\eta} 6 \times 10^{-9} M_{\odot}/yr$. To capture this much stellar wind matter, as shown in Extended Data Figure 4, the black hole mass must be greater than $46M_{\odot}$ for $\eta = 0.06$ in the case of a non-spinning Schwarzschild black hole, and greater than $13M_{\odot}$ for $\eta = 0.42$ in the case of a maximally spinning Kerr black hole. If we use the velocity law $v(r) = v_{\infty}(1 - R_{*}/r)^{\beta}$ with $\beta = 1$ for the inner wind¹⁶, then the black hole mass must be greater than $28M_{\odot}$ for $\eta = 0.06$ in the case of a non-spinning Schwarzschild black hole, and greater than $8M_{\odot}$ for $\eta = 0.42$ in the case of a maximally spinning Kerr black hole. If we adopt a typical η value of 0.1, the required accretion rate corresponds to $M_{\bullet} > 24M_{\odot}$ (and $i < 17^{\circ}$) for a wind velocity of $v \simeq 1100$ km s⁻¹, and corresponds to $M_{\bullet} > 32M_{\odot}$ (and $i < 14^{\circ}$) for the terminal velocity. The accretion rate argument thus requires a black hole of $> 8 - 46M_{\odot}$, likely a black hole of $20 - 30M_{\odot}$ similar to IC 10 X-1 and NGC 300 X-1.

The recurring X-ray/optical outbursts dictates the presence of an accretion disk prone to instability, and the disk formation under stellar wind accretion places stringent constraints on the binary system. To explore why the number of Galactic X-ray stars is so small, it has been shown⁴⁴ that in the case of accretion of stellar wind matter in a detached binary system the specific angular momentum of the matter captured by the compact object is typically small. Therefore, usually no accretion disk is formed around the compact object. Consequently, very special conditions are required for a black hole in a detached binary system to be a strong X-ray source. A disk may form

if the specific angular momentum of accreting matter, $Q_{acc} = \frac{1}{4} \frac{2\pi}{P} r_{acc}^2$, exceeds the specific angular momentum of the particle at the innermost stable circular orbit, $Q_{ISCO} = \sqrt{3} r_g c = \sqrt{3} \frac{2GM_\bullet}{c^2} c$. This is usually expressed as $P < 4.8 \frac{M_\bullet/M_\odot}{v_{1000}^4} \delta^2$ hr, where $\delta \sim 1$ is a dimensionless parameter^{19,45}. Given $P = 8.24 \pm 0.1$ days and $v_\infty = 1300 \pm 100$ km s⁻¹ for M101 ULX-1, the black hole mass is required to be $M_\bullet > 80M_\odot$, corresponding to $i = 9^\circ$ (i.e., nearly face-on). If the wind velocity from the velocity model of the inner wind¹⁶ is adopted, then the black hole mass is required to be $M_\bullet > 48M_\odot$, corresponding to $i = 11^\circ$.

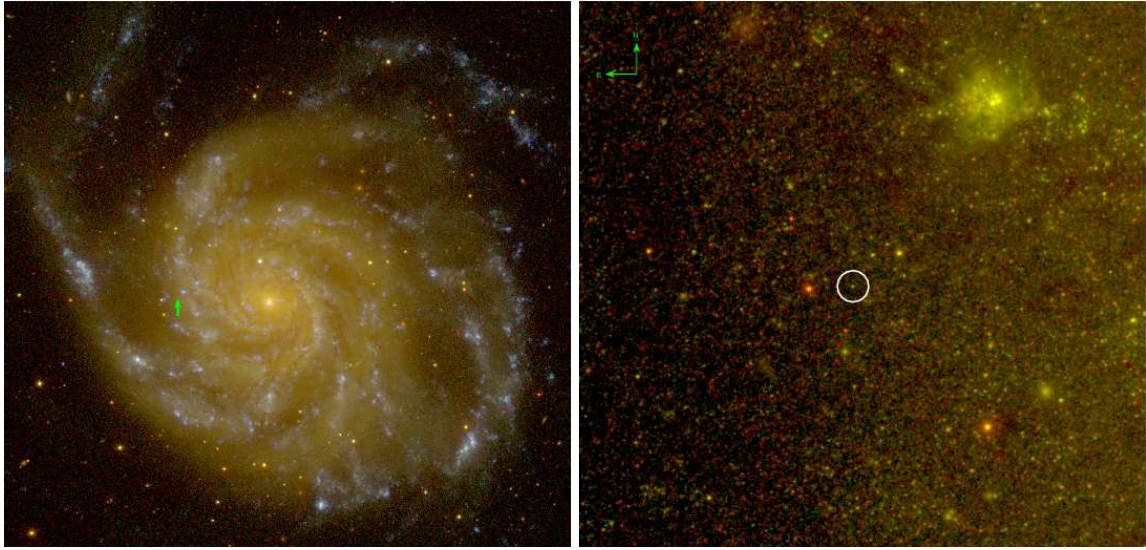
To investigate the possible presence of partial ionization zone, we need to compute the temperature structure $T_d(r)$ for the accretion disk, especially for the outer disk. Following the procedures designed for an X-ray irradiated black hole binary model for ULXs⁴⁶, we compute the disk temperature structure for a standard accretion disk with the α prescription⁴⁷ plus X-ray irradiation⁴³. As shown in Extended Data Figure 5, regardless of the black hole mass for M101 ULX-1, its outer disk temperature is as low as 4000K in the low-hard state due to its large separation and large disk, and the helium partial ionization zone at about 15000K is bound to exist unless the black hole mass is lower than $5.5M_\odot$. In comparison, the disk temperature for NGC 300 X-1, with an orbital period of 32.8 hrs and its WN5 star ($M_* = 26M_\odot$, $R_* = 7.2R_\odot$) filling its Roche lobe²², never drops below 20000K due to its small separation and small disk, and there is no helium partial ionization zone in the disk. This explains naturally why NGC 300 X-1 and similar IC 10 X-1 exhibit steady X-ray radiation despite the apparent variations due to orbital modulation under the edge-on viewing geometry.

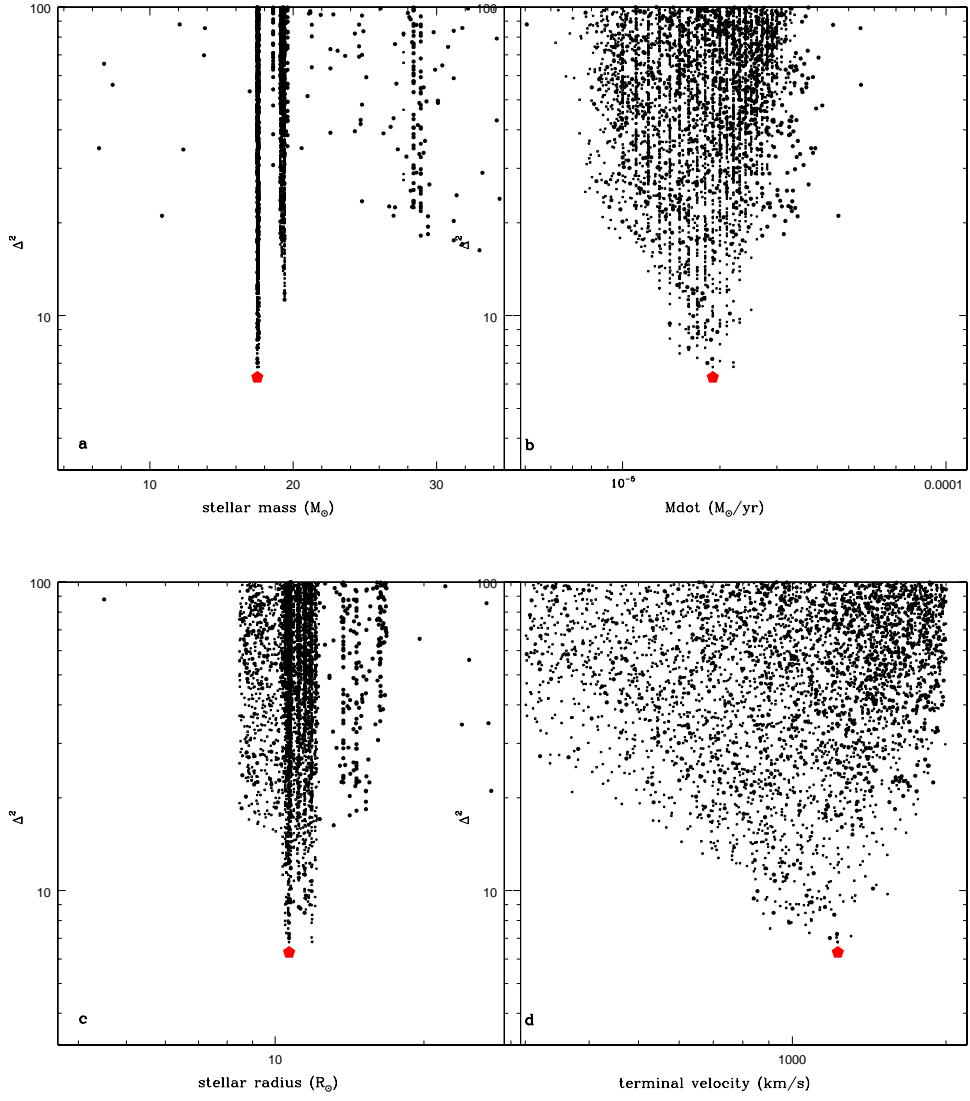
The existence of an accretion disk in M101 ULX-1 is also supported by the observed spectral state changes, which resemble those for Galactic black hole binaries^{9,11} that are believed to reflect changes in the properties of their accretion disks¹⁰. During its outbursts, M101 ULX-1 exhibits an X-ray spectrum^{4,7} that can be classified as a thermal dominant state (albeit with exceptionally low disk temperatures), a well-defined spectral state that corresponds to a standard thin accretion disk at about 10% of its Eddington luminosity. Quantitative studies²³ show that when the luminosity exceeds 30% of the Eddington limit, the emission changes such that the X-ray spectrum includes a steep power-law with a significant hard component above 2 keV. The presence of such a hard component is not seen in the X-ray spectra of M101 ULX-1. Given its bolometric luminosity of $3 \times 10^{39} \text{ erg s}^{-1}$ in the thermal dominant state at less than 30% of its Eddington limit, we infer that the black hole mass is above $80M_{\odot}$. If this is true, the inferred black hole mass of M101 ULX-1 may challenge the expectations of current black hole formation theories. The most massive black holes that can be produced for solar metallicity are about $15M_{\odot}$, and about $20M_{\odot}$ ($25M_{\odot}$, $30M_{\odot}$) for $0.6\times$ ($0.4\times$, $0.3\times$) solar metallicity due to reduced stellar winds and hence reduced mass loss in the final stages before stellar collapse⁴⁸.

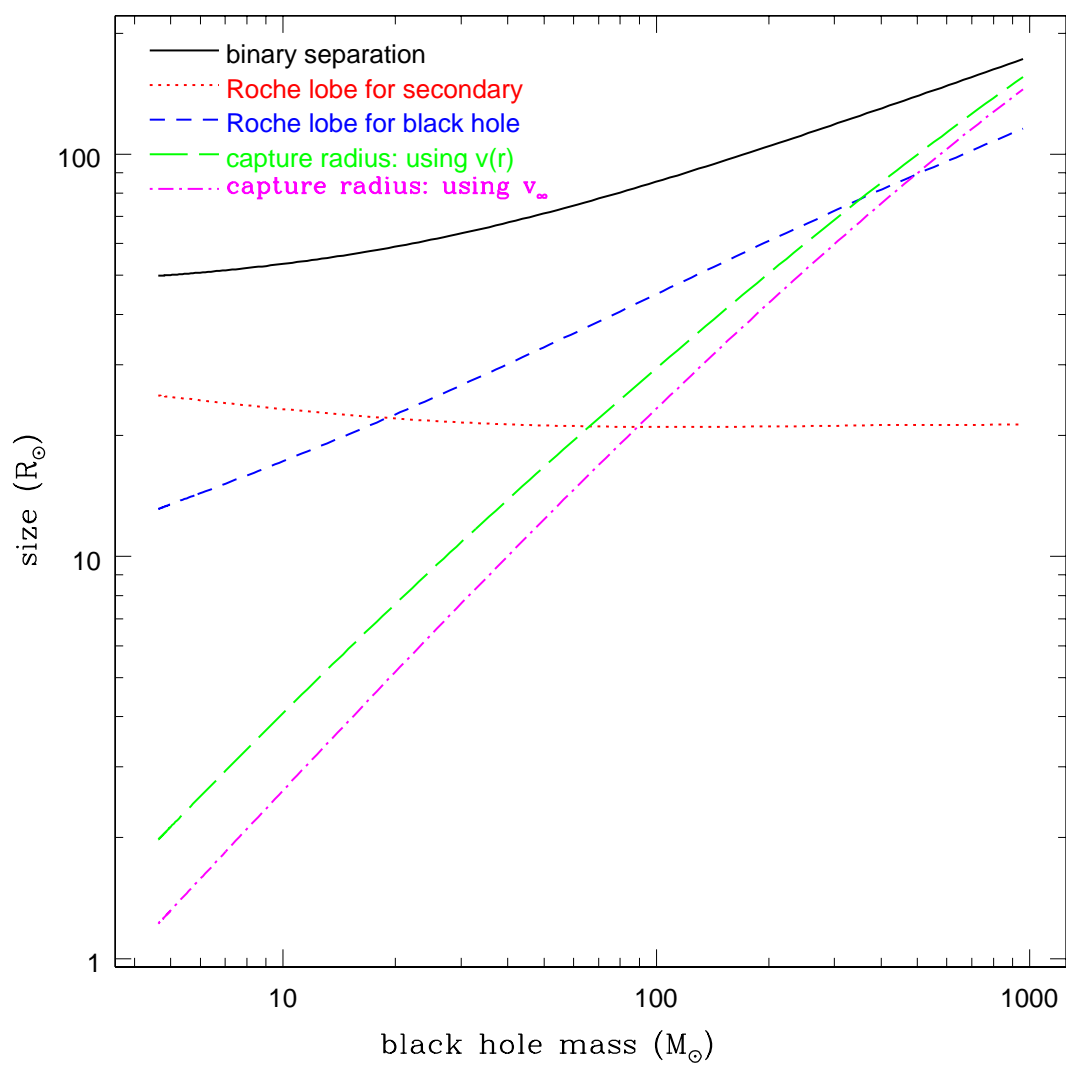
31. Freedman, W. *et al.* Final results from the Hubble Space Telescope key project to measure the Hubble Constant, *Astrophys. J.* **553**, 47-72 (2001)
32. Kong, A. K. H., Rupen, M. P., Sjouwerman, L. O. & Di Stefano, R. *Proceedings Papers of the 22nd Texas Symposium on Relativistic Astrophysics at Stanford*. (Stanford Univ. 2005)
33. Bresolin, F. The oxygen abundance in the inner H II regions of M101: implications for the

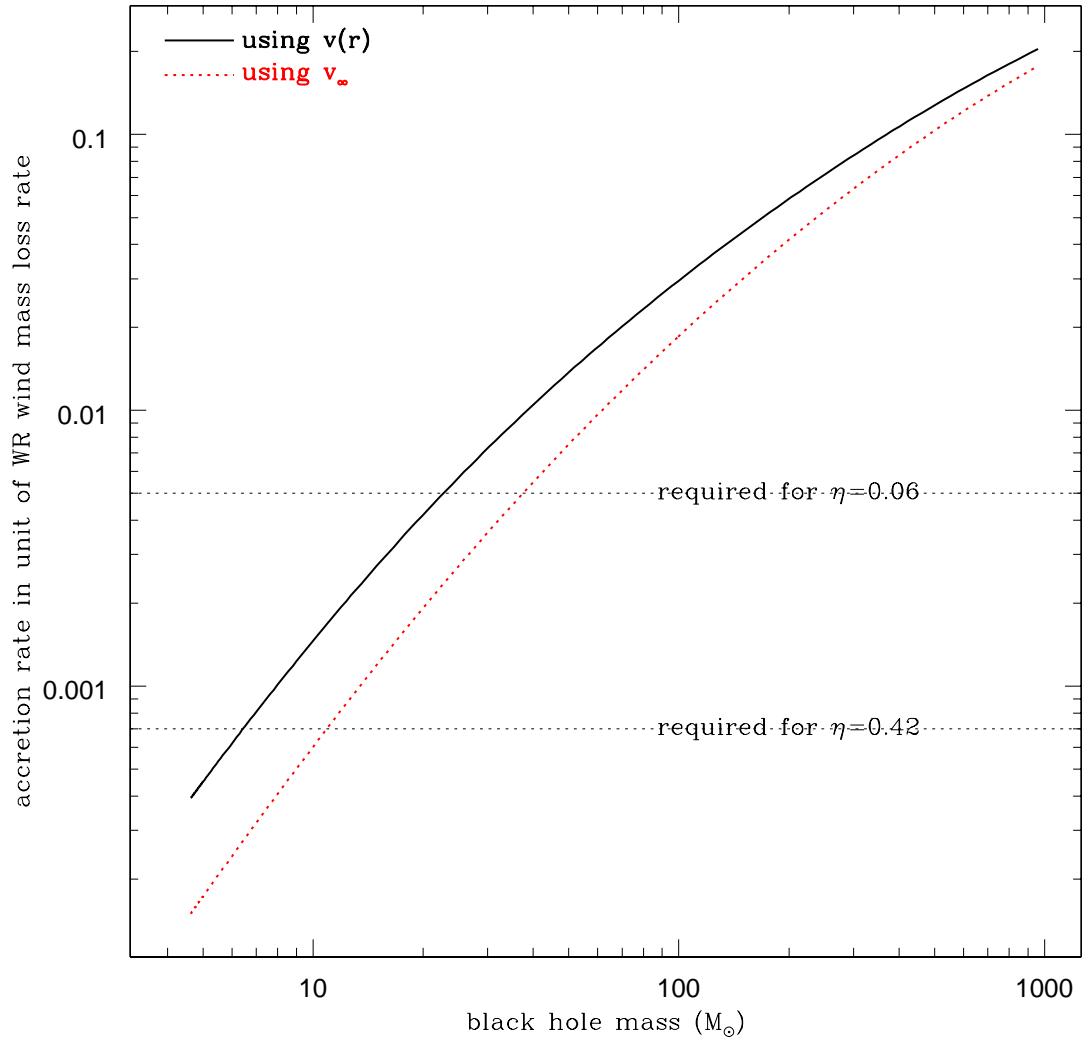
- calibration of strong-line metallicity indicators. *Astrophys. J.* **656**, 186-197 (2007)
34. Liu, J. F. Chandra ACIS survey of X-ray point sources in 383 nearby galaxies. I. The source catalog. *Astrophys. J.* **192** (suppl.). 10-64 (2011)
 35. Kong, A. K. H. & Di Stefano, R. An unusual spectral state of an ultraluminous very soft X-ray source during outburst. *Astrophys. J.* **632**, L107-L110 (2005)
 36. Kuntz, K. D. *et al.* The optical counterpart of M101 ULX-1. *Astrophys. J.* **620**, L31-L34 (2005)
 37. Pettini, M. & Pagel, B. E. J. [OIII]/[NII] as an abundance indicator at high redshift. *Mon. Not. R. Astron. Soc.* **348**, L59-L63 (2004)
 38. Osterbrock, D. *Astrophysics of Gaseous Nebulae and Active Galactic Nuclei*. (University Science Books 1989)
 39. Hamann, W. R., Koesterke, L. & Wessolowski, U. Spectra analysis of the Galactic Wolf-Rayet stars - a comprehensive study of the WN class. *Astron. Astrophys.* **274**, 397-414 (1993)
 40. Crowther, P. A. & Hadfield, L. J. Reduced Wolf-Rayet line luminosities at low metallicity. *Astron. Astrophys.* **449**, 711-722 (2006)
 41. Smith, L. F., Shara, M. M. & Moffat, A. F. J. A three-dimensional classification for WN stars. *Mon. Not. R. Astron. Soc.* **281**, 163-191 (1996)
 42. Girardi, L. *et al.* Theoretical isochrones in several photometric systems. I. Johnson-Cousins-Glass, HST/WFPC2, HST/NICMOS, Washington, and ESO imaging survey filter sets. *Astron. Astrophys.* **391**, 195-212 (2002)

43. Frank, J., King, A. & Raine, D. *Accretion Power in Astrophysics*. (Cambridge Univ. Press, 2002)
44. Illarionov, A. F. & Sunyaev, R. A. Why the number of Galactic X-ray stars is so small? *Astron. Astrophys.* **39**, 185-195 (1975)
45. Ergma, E. & Yungelson, L. R. CYG X-3: can the compact object be a black hole? *Astron. Astrophys.* **333**, 151-158 (1998)
46. Liu J. F., Orosz, J. & Bregman, J. N. Dynamical mass constraints on the ultraluminous X-ray source NGC 1313 X-2. *Astrophys. J.* **745**, 89-110 (2012)
47. Shakura, N. I. & Sunyaev, R. A. Black holes in binary systems. Observational appearance. *Astron. Astrophys.* **24**, 337-355 (1973)
48. Belczynski, K. *et al.* On the maximum mass of stellar black holes. *Astrophys. J.* **714**, 1217-1226 (2010)









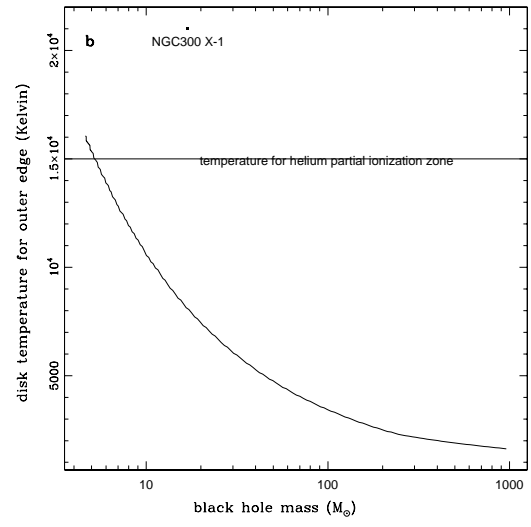
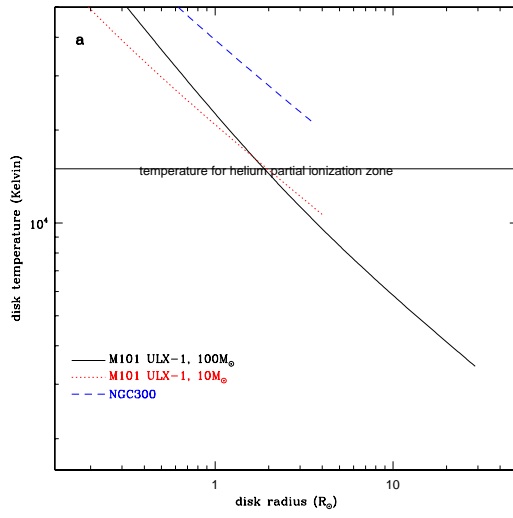


Table 1: Gemini/GMOS spectroscopic observations of M101
ULX-1

OBSDATE	MJD	exposure (second)	bary. (km/s)	velocity (km)
2010-02-15	55242.58343	3200	7.4	212
2010-02-16	55243.50615	3200	7.3	236
2010-03-16	55271.54390	3200	0.1	301
2010-03-17	55272.54564	3200	-0.2	—
2010-04-17	55303.47547	4800	-7.7	326
2010-05-13	55329.33126	6400	-12.2	302
2010-05-14	55330.39682	6400	-12.4	256
2010-05-15	55331.37803	6400	-12.5	227
2010-05-18	55334.41410	9600	-13.0	244
2010-05-19	55335.42391	9600	-13.1	305

The columns are: (1) Observation date, (2) Modified Julian Date, (3) exposure time in seconds, (4) barycentric correction computed with `rvsao`, and (5) the corrected radial velocity as measured with Hell 4686, with an error of 15 km/s as mainly from the uncertainties in the wavelength calibration.

Table 2: Properties of emission lines

Line	FWHM	E.W.	Lum.	model
ID	(Å)	(Å)	10^{34} erg/s	(Å)
HeII 4686	19.3	21.83 ± 0.20	43	21.75
HeI 5876	19.0	34.78 ± 0.29	49	34.21
HeI 6679	18.8	25.74 ± 0.37	24	26.56
HeII 5411	20.5	5.46 ± 0.13	8.3	6.10
HeI 4922	13.4	5.80 ± 0.64	8.4	3.91
HeI 4471	12.1	3.86 ± 0.65	7.0	5.18
H_γ	3.6	1.35 ± 0.22	2.7	
H_β	4.5	7.51 ± 0.06	12	
H_α	4.7	26.54 ± 0.46	34	
[OIII] 4960	4.4	23.70 ± 0.49	40	
[NII] 6548	3.8	3.85 ± 0.39	4.7	
[NII] 6583	4.7	16.66 ± 0.08	18	
[SII] 6716	4.0	4.58 ± 0.07	4.0	
[SII] 6731	4.6	3.81 ± 0.06	3.1	

The columns are: (1) emission line ID, (2) FWHM as obtained from Gaussian fit, which equals to 2.35σ , (3) equivalent width, (4) line luminosity in unit of 10^{34} erg/s, and (5) equivalent width from the best WR synthetic model.

Figure 1 M101 ULX-1 as observed in the optical. (a) M101 ULX-1 is located on a spiral arm of the face-on grand-design spiral galaxy M101, as indicated by the arrow. The color image of M101 is composed of GALEX NUV, SDSS g, and 2MASS J images. (b) ULX-1 is identified as a blue object with $V=23.5$ mag at the center of the $1''$ circle on the HST image. The color image is composed of ACS/WFC F435W, F555W and F814W images.

Figure 2 Physical properties of the WR secondary from spectral line modeling. Distributions of computed Δ^2 as a function of (a) stellar masses, (b) stellar mass loss rate, (c) stellar radii, and (d) terminal velocity. Here $\Delta^2 = \sum_i (EW - EW_i)^2$ computes the difference between observed and synthetic equivalent widths for six broad helium lines present in the Gemini/GMOS spectrum. We have computed synthetic spectra for a group of 5000 real stars from the evolution tracks (as shown by the thick stripes in the mass plot and the radius plot) and for another group of "fake" stars with continuous distributions in mass, radius and luminosity. The best model is labeled by a filled pentagon in all panels.

Figure 3 Properties for the Wolf-Rayet/black hole binary for different black hole masses. Properties for the Wolf-Rayet/black hole binary for different black hole masses. Shown are the binary separation (solid), the Roche lobe sizes for the Wolf-Rayet star (dotted) and for the black hole (dashed), the capture radius for the black hole when using the terminal velocity (dash-dotted) or when using a simplified velocity law $v(r) = v_\infty(1 - R_*/r)$ (long-short dashed).

Figure 4 The black hole accretion rate for different black hole mass. The black hole accretion rate for different black hole mass if adopting the terminal velocity (dotted) or a simplified velocity law $v(r) = v_\infty(1 - R_*/r)$ (solid). To power the observed average luminosity of 3×10^{38} erg/s, the black hole mass must exceed $13M_\odot$ ($8M_\odot$) using the terminal velocity (the velocity law) for a Kerr black hole, and exceed $46M_\odot$ ($28M_\odot$) for a Schwarzschild black hole.

Figure 5 Disk temperature structures for M101 ULX-1. (a) The disk temperature profiles for M101 ULX-1 (for $P = 8.24\text{days}$, $M_* = 19M_\odot$, $R_* = 10.7R_\odot$, $M_\bullet = 10/100M_\odot$) and NGC300 X-1 (for $P = 32.4\text{hr}$, $M_* = 26M_\odot$, $R_* = 7.2R_\odot$, $M_\bullet = 16.9M_\odot$; Crowther et al. 2010). (b) The disk temperature at the outer edge for different black hole mass in M101 ULX-1.